A USER FRIENDLY SYSTEM, HIGH EFFICIENT BOOST CONVERTER WITH COUPLED INDUCTOR MULTIPHASE TOPOLOGY FOR PHOTOVOLTAIC MODULE

Mohd Abdul Kareem*

Mohammed Abdul Rahman Uzair**

Masarath Unnisa*

Ishrath Jahan*

***Abstract*— Within the photovoltaic (PV) power-generation market, the PV module has shown obvious growth. However, a high voltage gain converter is essential for the module's grid connection through a DC–ac inverter. This paper proposes a converter that employs a floating active switch to isolate energy from the PV panel when the ac module is OFF; this particular design protects installers and users from electrical hazards and acts as a user friendly system. Without extreme duty ratios and the numerous turns-ratios of a coupled inductor, this converter achieves a high step-up voltage-conversion ratio; the leakage inductor energy of the coupled inductor is efficiently recycled to the load. These features explain the module's high-efficiency performance. The detailed operating principles and steady-state analyses of continuous, discontinuous, and boundary conduction modes are described. A 15V input voltage, 200V output voltage, and 100W output power prototype circuit of the proposed converter has been implemented; its maximum efficiency is up to 95.3% and full-load efficiency is 92.3%.**

Keywords: PV module, Continuous Conduction Mode (CMM), DC-DC Converter, CIMP technique, Active switch.

* Assistant Professor, Nawab Shah Alam Khan College of Engg and Tech, Malakpet - Hyderabad, T.S., INDIA.

** Associate Professor, Nawab Shah Alam Khan College of Engg and Tech, Malakpet - Hyderabad, T. S., INDIA.

I. INTRODUCTION

In recent years, there has been an upsurge of interest in solar photovoltaic (PV) energy systems in both industry and academia. In typical PV power generation systems, several photovoltaic panels are connected in series and parallel to form an array and feed energy to a single centralized inverter or to a few parallel 'string' inverters. An alternative approach is to use an AC module, which is a combination of one PV panel and one power conditioning unit, to feed power directly into the grid.

The advantages of an AC module based system over systems based on centralized inverter or parallel string inverters are as follows:

1) The maximum power point (MPP) of each panel can be tracked individually, thereby increasing the utilization of the whole PV system;

2) Detrimental effects due to shading and module mismatches are not present.

3) Potential arcing problems due to DC system wiring are fully avoided.

4) The "plug and play" property allows easy system expansion through simple paralleling of additional AC modules.

However, an AC module based system has a few problems also, including potential reduction in system efficiency and possible cost increase in the overall system cost due to the use of several low power inverters. Greater maintenance may also be required, though overall reliability may actually improve due to the use of several parallel inverters. Among the variety of circuits and control methods that have been developed for the AC module application, the flyback DCM (discontinuous conduction mode) inverter is one of the favored topologies because of its simplicity and potential low cost. The component count is low and the inverter requires only a simple control scheme.

II. PHOTOVOLTAIC TECHNOLOGY

Photovoltaic is the field of technology and research related to the devices which directly convert sunlight into electricity. The solar cell is the elementary building block of the photovoltaic technology. Solar cells are made of semiconductor materials such as silicon. One of the properties of semiconductors that makes them most useful is that their conductivity may easily be modified by introducing impurities into their crystal lattice [1].

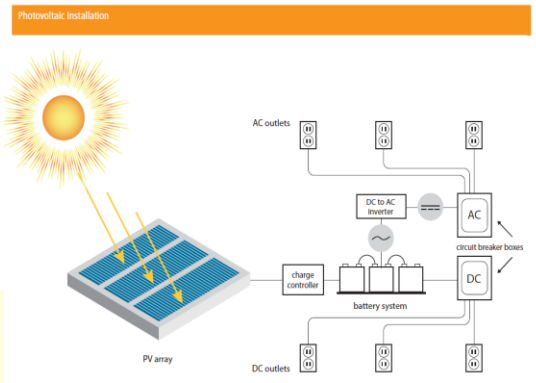

Figure1: photovoltaic installation

III. PROPOSED CONCEPT

Photovoltaic (PV) power-generation systems are becoming increasingly important and prevalent in

distribution generation systems. A conventional centralized PV array is a serial connection of numerous panels to obtain higher DC-link voltage for main electricity through a DC–AC inverter. The total power generated from the PV array is sometimes decreased remarkably when only a few modules are partially covered by shadows, thereby decreasing inherent current generation, and preventing the generation current from attaining its maximum value on the array. To overcome this drawback, an ac module strategy has been proposed. In this system, a low-power DC–ac utility interactive inverter is individually mounted on PV module and operates so as to generate the maximum power from its corresponding PV module as in Fig. 2 below.

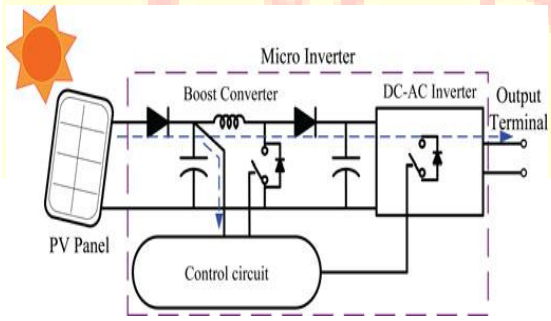

Figure2: Potential difference on the output terminal of non floating switch Micro inverter

The power capacity range of a single PV panel is about 100W to 300W, and the maximum power point (MPP) voltage range is from 15V to 40V, which will be the input voltage of the ac module [2]; in cases with lower input voltage, it is difficult for the ac module to reach high efficiency. However, employing a high step-up DC–DC converter in the front of the inverter improves power-conversion efficiency and provides a

stable DC link to the inverter. The micro inverter includes DC–DC boost converter, DC–ac inverter with control circuit as shown in Fig. 1. The DC–DC converter requires large step-up conversion from the panel's low voltage to the voltage level of the application. The DC-input converter must boost the 48 V of the DC bus voltage to about 380–400 V. Generally speaking, the high step-up DC–DC converters for these applications have the following common features:

1) High step-up voltage gain. Generally, about a tenfold step-up gain is required.

2) High efficiency.

3) No isolation is required [3].

There are two major concerns related to the efficiency of a high step-up DC–DC converter: large input current and high output voltage.

Fig. 1 shows the solar energy through the PV panel and micro inverter to the output terminal when the switches are OFF [4]. When installation of the ac module is taking place, this potential difference could pose hazards to both the worker and the facilities. A floating active switch is designed to isolate the DC current from the PV panel, for when the ac module is off-grid as well as in the non operating condition. This isolation ensures the operation of the internal components without any residential energy being transferred to the output or input terminals, which could be unsafe.

IV. OPERATING PRINCIPLES OF THE PROPOSED CONVERTER

The simplified circuit model of the proposed converter is shown in Fig. 3. The coupled inductor T_1 is represented as a magnetizing inductor *Lm*, primary and secondary leakage inductors L_{k1} and L_{k2}, and an ideal transformer. In order to simplify the circuit analysis of the proposed converter, the following assumptions are made.

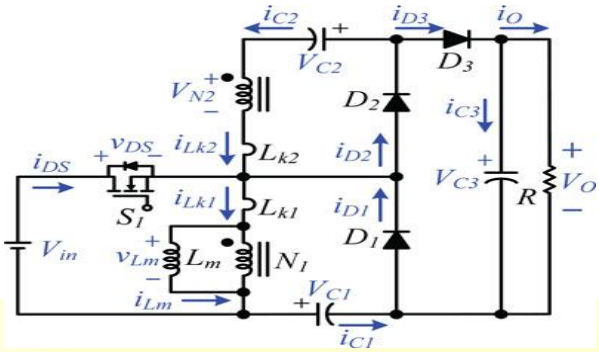

Figure3: Polarity definitions of voltage and current in proposed converter

1) All components are ideal, except for the leakage inductance of coupled inductor T_1, which is being taken under consideration. The on-state resistance R_{DS}(ON) and all parasitic capacitances of the main switch S_1 are neglected, as are the forward voltage drops of diodes $D_1 \sim D_3$.

2) The capacitors $C_1 \sim C_3$ are sufficiently large that the voltages across them are considered to be constant.

3) The ESR of capacitors $C_1 \sim C_3$ and the parasitic resistance of coupled inductor T_1 are neglected.

4) The turns ratio n of the coupled inductor T_1 windings is equal to N_2 / N_1. The operating principle of continuous conduction mode (CCM) is presented in detail. The current waveforms of major components are given in Fig. 3.4. There are five operating modes in a switching period. The operating modes are described as follows.

A) CCM Operation

Mode I [t_0, t_1]: In this transition interval, the magnetizing inductor L_m continuously charges capacitor C_2 through T_1 when S_1 is turned ON. The current flow path is shown in Fig. 5(a); switch S_1 and diode D_2 are conducting. The current i_{Lm} is decreasing because source voltage V_{in} crosses magnetizing inductor Lm and primary leakage inductor L_{k1}; magnetizing inductor L_m is still transferring its energy through coupled inductor T_1 to charge switched capacitor C_2, but the

energy is decreasing; the charging current i_{D2} and i_{C2} are decreasing. The secondary leakage inductor current i_{LK2} is declining as equal to i_{Lm} / n. Once the increasing i_{Lk1} equals decreasing i_{Lm} at $t = t1$, this mode ends.

Mode II [t_1, t_2]: During this interval, source energy Vin is series connected with N_2 , C_1 and C_2 to charge output capacitor C_3 and load R; meanwhile magnetizing inductor L_m is also receiving energy from V_{in} . The current flow path is shown in Fig. 5(b), where switch S_1 remains ON, and only diode D_3 is conducting. The i_{Lm}, i_{Lk1} , and $iD3$ are increasing because the V_{in} is crossing L_{k1} , L_m, and primary winding N_1 ; L_m and L_{k1} are storing energy from V_{in} ; meanwhile V_{in} is also serially connected with secondary winding N_2 of coupled inductor.

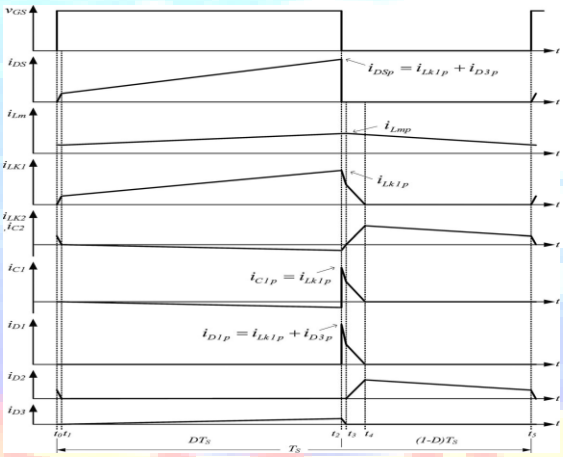

Figure4: Some typical waveforms of proposed converters at CCM operation

T_1, capacitors C_1 , and C_2 , and then discharges their energy to capacitor C_3 and load R. The i_{in} , $i_{D\,3}$ and discharging current $|iC1|$ and $|iC2|$ are increasing. This mode ends when switch S_1 is turned OFF at $t = t_2$.

Mode III [t_2 , t_3]: During this transition interval, secondary leakage inductor L_{k2} keeps charging C_3 when switch S_1 is OFF. The current flow path is shown in Fig. 5(c), where only diode D_1 and D_3 are conducting. The energy stored in leakage inductor L_{k1} flows through diode D_1 to charge capacitor C_1 instantly when S_1 is OFF. Meanwhile, the energy of secondary leakage inductor L_{k2} is series connected with C_2 to charge output capacitor C_3 and the load. Because leakage inductance L_{k1} andL_{K2} are far smaller than L_m, i_{Lk2} rapidly decreases, but i_{Lm} is increasing

because magnetizing inductor L_m is receiving energy from L_{k1} . Current i_{Lk2} decreases until it reaches zero; this mode ends at $t = t_3$.

Mode IV [t_3,t_4]: During this transition interval, the energy stored in magnetizing inductor L_m is released to C_1 and C_2 simultaneously. The current flow path is shown in Fig. 5(d). Only diodes D_1 and D_2 are conducting. Currents i_{Lk1} and i_{D1} are continually decreased because the leakage energy still flowing through diode D_1 keeps charging capacitor C_1. The L_m is delivering its energy through T_1 and D_2 to charge capacitor C_2 . The energy stored in capacitor C_3 is constantly discharged to the load R. These energy transfers result in decreases in i_{Lk1} and i_{Lm} but increases in i_{Lk2} . This mode ends when current i_{Lk1} is zero, at $t = t_4$.

Mode V [t_4,t_5]: During this interval, only magnetizing inductor L_m is constantly releasing its energy to C_2 . The current flow path is shown in Fig. 5(e), in which only diode D_2 is conducting. The i_{Lm} is decreasing due to the magnetizing inductor energy flowing through the coupled inductor T_1 to secondary winding N_2 and D_2 continues to charge capacitor C_2. The energy stored in capacitor C_3 is constantly discharged to the load R. This mode ends when switch S_1 is turned ON at the beginning of the next switching period.

B) DCM Operation

The detailed operating principles for discontinuous conduction- mode (DCM) operation are presented in this section. Fig. 6 depicts several typical waveforms during five operating modes of one switching period. The operating modes are described as follows.

Mode I [t_0,t_1]: During this interval, source energy V_{in} is series connected with N_2 , C_1 and C_2 to charge output capacitor C_3 and load R; meanwhile, magnetizing inductor L_m is also receiving energy from V_{in} . The current flow path is shown in Fig. 7(a), which depicts that switch S_1 remains ON, and only diode D_3 is conducting. The $i_{Lm,}$ i_{Lk1} , and i_{D3} are increasing because the V_{in} is crossing L_{k1} , L_m, and primary winding N_1 ; L_m and L_{k1} are storing energy from V_{in} ; meanwhile, V_{in} also is serially connected with secondary winding N_2 of coupled inductor T_1 , capacitors C_1 , and C_2 ; then they all discharge their energy to capacitor C_3 and load R. The i_{in} , i_D

$_3$ and discharging current $|iC1|$ and $|iC2|$ are increasing. This mode ends when switch S_1 is turned OFF at $t = t_1$.

Mode II [t_1,t_2]: During this transition interval, secondary leakage inductor L_{k2} keeps charging C_3 when switch S_1 is OFF. The current flow path is shown in Fig. 7(b), and only diode D_2 and D_3 are conducting. The energy stored in leakage inductor L_{k1} flows through diode D_1 to charge capacitor C_1 instantly when S_1 is OFF. Meanwhile, the energy of secondary leakage inductor L_{k2} is series-connected with C_2 to charge output capacitor C_3 and the load. Because leakage inductance L_{k1} and L_{K2} are far smaller than L_m, i_{Lk2} decreases rapidly, but i_{Lm} is increasing because magnetizing inductor L_m is receiving energy from L_{k1} . Current i_{Lk2} reduces down to zero, and this mode ends at $t = t_2$.

Mode III [t_2,t_3]: During this transition interval, the energy stored in coupled inductor T_1 is releasing to C_1 and C_2. The current flow path is shown in Fig.7(c). Only diodes D_1 and D_2 are conducting. Currents i_{Lk1} and i_{D1} are continually decreased because leakage energy still flowing through diode D_1 keeps charging capacitor C_1. The L_m is delivering its energy through T_1 and D_2 to charge capacitor C_2 .The energy stored in capacitor C_3 is constantly discharged to the load R. These energy transfers result in decreases in i_{Lk1} and i_{Lm} but increases in $i_{Lk2.}$ This mode ends when current i_{Lk1} reaches zero at $t = t_3$.

Mode IV [t_3,t_4]: During this interval, only magnetizing inductor L_m is constantly releasing its energy to C_2 . The current flow path is shown in Fig.7(d), and only diode$D2$ is conducting.

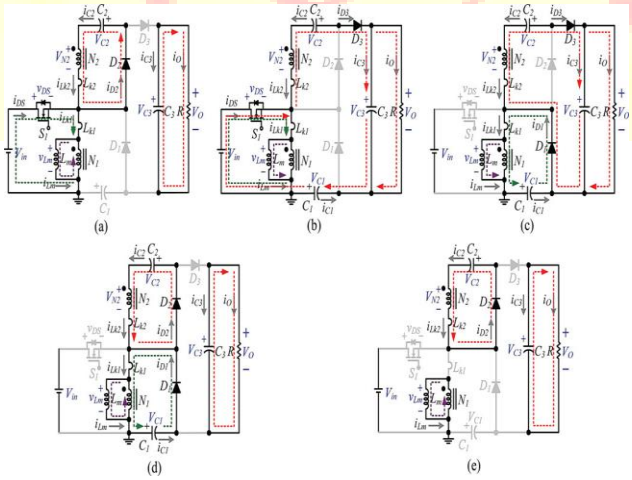

Figure5: CCM operation modes

(a) Mode I: $t_0 \sim t_1$; (b) Mode II: $t_1 \sim t_2$; (c) Mode III: $t_2 \sim t_3$; (d) Mode IV: $t_3 \sim t_4$; (e) Mode V: $t_4 \sim t_5$

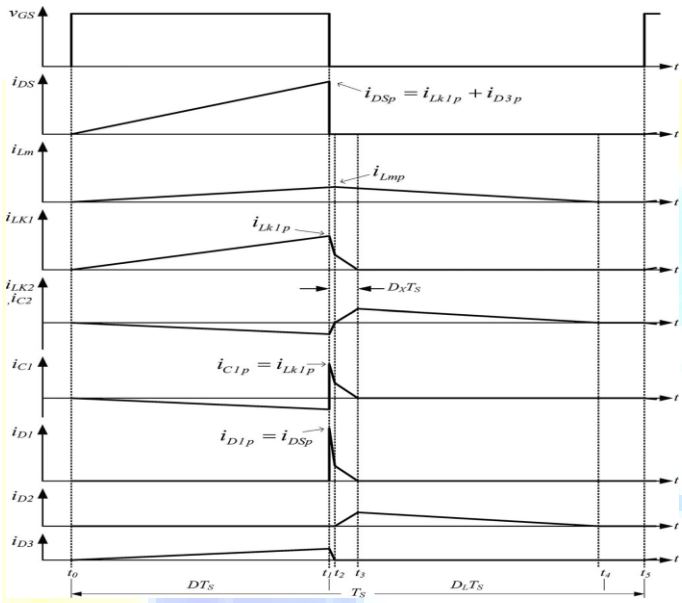

Figure6: Some typical waveforms of proposed converters at DCM operation

The i_{Lm} is decreasing due to the magnetizing inductor energy flowing through the coupled inductor T_1 to secondary winding N_2 , and D_2 continues to charge capacitor C_2 . The energy stored in capacitor C_3 is constantly discharged to the load R. This mode ends when current i_{Lm} reaches zero at $t = t_4$.

Mode V [t_4,t_5]: During this interval, all active components are turned OFF; only the energy stored in capacitor C_3 is continued to be discharged to the load R. The current flow path is shown in Fig. 7(e). This mode ends when switch S_1 is turned ON at the beginning of the next switching period.

V. STEADY-STATE ANALYSIS OF PROPOSED CONVERTERS

A) CCM Operation

To simplify the steady-state analysis, only modes II and IV are considered for CCM operation, and the leakage inductances on the secondary and primary sides are neglected. The following equations can be written from Fig. 5(b):

$v_{Lm}=V_{in}$ *(1)*

$V_{N2}=nV_{in}$ *(2)*

During mode IV

$v_{Lm} = -VC1$ *(3)*

$v_{N2} = -VC2$ *(4)*

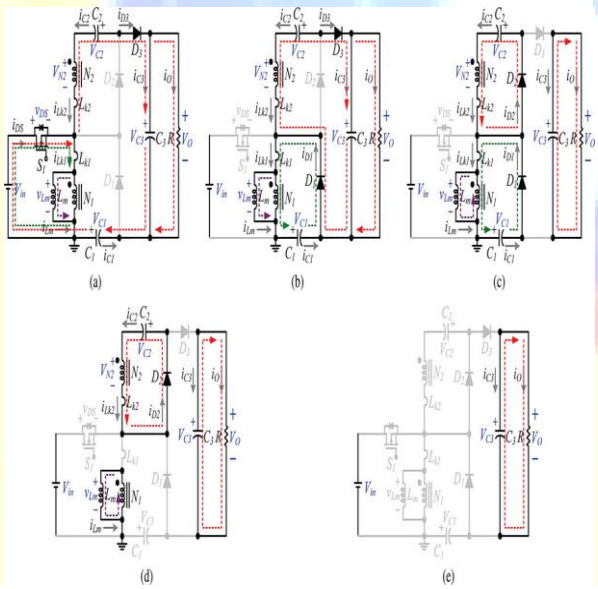

Figure7: DCM operation modes

(a) Mode I: $t_0 \sim t_1$; (b) Mode II: $t_1 \sim t_2$; (c) Mode III: $t_2 \sim t_3$; (d) Mode IV: $t_3 \sim t_4$; (e) Mode V: $t_4 \sim t_5$

Applying a volt-second balance on the magnetizing inductor *Lm* yields

$$\int_0^{DTS}(Vin)dt + \int_{DTS}^{(D+DL)TS}(-Vc1)dt = 0 \qquad (5)$$

$$\int_0^{DTS}(nVin)dt + \int_{DTS}^{(D+DL)TS}(-VC2)dt = 0 \qquad (6)$$

From which the voltage across capacitors$C1$ anDC2 are obtained as follows:

$V_{c1}=DV_{in}/(1-D)$ (7)

$V_{c2}=nDV_{in}/(1-D)$ (8)

During mode II, the output voltage

$V_O = V_{\text{in}} + V_{N\,2} + V_{C\,2} + V_{C\,1}$ becomes

$V_o=V_{in}+nV_{in}+nDV_{in}/[1-D]+DV_{in}/[1-D]$ (9)

The DC voltage gain MCCM can be found as follows:

$M_{CCM}=(V_o/V_{in})=(1+n)/(1-D)$ (10)

Both [10] and [11] are employing coupled inductor topology as the boost type converter integrating with coupled inductor; this technology is similar to the technology of the proposed converter. Fig. 8 shows the plot of voltage gain *M*CCM as function of duty ratio *D* of the proposed converter is compared with that and under CCM operation and n = 5 of available converters. The chart reveals the voltage gain CCM of proposed converter is obviously higher than available converters.

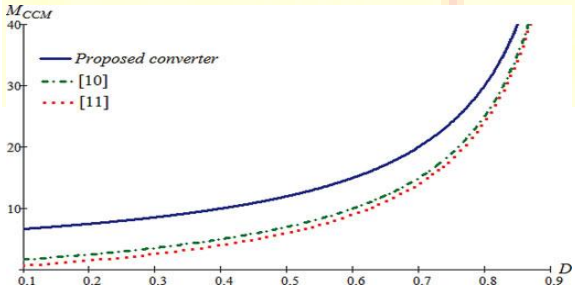

Figure8: Voltage gain as a function of the duty ratio of the proposed converter

All of them are operating under the same conditions: CCM and n = 5. During CCM operation, the voltage stresses on S_1 and D_1~D_3 are given as

$V_{DS}=V_{D1}=(V_{in}/1-D)$ (11)

$V_{D2}=(nV_{in}/1-D)$ (12)

$V_{D3}=(1+n)V_{in}/1-D$ (13)

B) DCM Operation

To simplify the steady-state analysis, only modes I and IV are considered for DCM operation, and the leakage inductances on the secondary and primary sides are neglected. The following equations can be written from Fig. 7(a). When switch *S*1 is turned ON, the voltage levels across inductors *Lm* and secondary winding *N*2 are

$V_{Lm}=V_{in}$ (14)

$v_{N2}=nVi_n$ (15)

When switch *S*1 is turned OFF, the voltage levels across inductors *Lm* and secondary winding *N*2 are

$v_{Lm}=-V_{c1}$ (16)

$-v_{N2}=V_{C2}$ (17) *DLTS* is the period of time during which current i_{Lm} declines from peak current to zero. The voltage across L_m and secondary winding N_2 can be found, as follows, by using the volt-second Balance principle

$$\int_0^{DTS}(Vin)dt+\int_{DTS}^{(D+DL)TS}(-Vc1)dt=0 \quad (18)$$

$$\int_0^{DTS}(nVin)dt+\int_{DTS}^{(D+DL)TS}(-VC2)dt=0 \quad (19)$$

Which derives the voltage of C_3 , C_4 , and output voltage as

$V_{C1}=DV_{in}/D_L$ *(20)*

$V_{C2}=nDV_{in}/D_L$ *(21)*

$Vo=(n+1)(D+DL)V_{in}/D_L$ *(22)*

Equation (22) yields D_L as follows:

$D_L= (n+1)D/[(V_o/V_{in})-(n+1)]$ *(23)*

Since the average currents of capacitor I_{C1} , I_{C2} , I_{C3} are zero in steady state, the average current values for I_{D3} , I_{D2} , and I_{D1} are, respectively, equal to the average value of I_O. The I_{Lmp} is the peak current of the magnetizing inductor, as shown in the following:

$I_{Lmp=}V_{In}DT_S/L_m$ *(24)*

From Fig. 6, the average values for $D1$ and $D2$ are derived as

$I_{D1}=(0.5)I_{Lmp}D_XT_s/Ts$ *(25)*

$I_O=I_{D2}=I_{Lmp}(D_L-D_X)T_S/2nT_S$ *(26)*

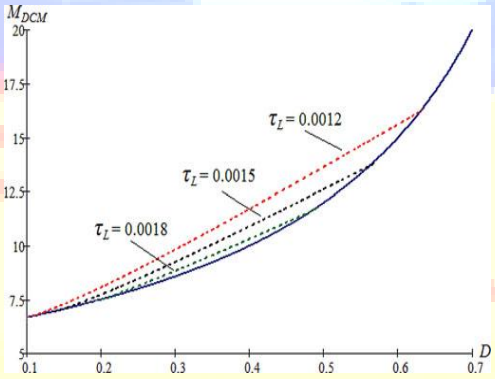

Figure9: Voltage gain as a function of the duty ratio of the proposed converter

DCM operates with different τ_L considering n = 5. Since the average current values for $I_{D\,2}$ and I_{D1} are, respectively, equal to the average value of I_O (25) is equal to (26),D_X , which is defined as the duration during which diode current i_{D1} travels from peak down to zero, is

$D_X=D_L/n+1$ *(27)*

Then, substituting (27) into (26), the *IO* can be rewritten as

$I_O=D_L I_{LMP}/2(n+1)$ *(28)*

Since *IO* = *VO* / *R*, substituting (24) and (27) into (28) yields

$2D/[(V_O/V_{IN})-(n+1)](V_{in}/V_O)D=L_m/RT_S$ (29)

The normalized magnetizing inductor time constant τL is defined as

$\tau_L=L_m/RTs=L_m f_s/R$ *(30)*

where f_S is the switching frequency. Substituting (30) into (29) obtains the voltage gain of the proposed converter in DCM, as follows:

$M_{DCM}=V_O/V_{in}=[(n+1)+\sqrt{(n+1)(n-1)+(\frac{2D(D)}{TL})}]/2$

……*(31)*

Equation (31) can be used to illustrate DCM voltage gain lines by different magnetizing inductor time constants $\tau_{L,}$ as shown in Fig. 9.

C) BCM Condition

When the proposed converter is operating in boundary conduction mode (BCM), the voltage gains of CCM and DCM operation are equal. Using (10) and (31) allows boundary

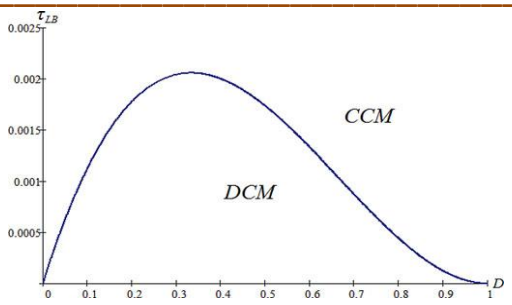

Figure10: Boundary condition of τ_{LB} of proposed converter under n = 5

$$T_{LB}=D(1-D)^2/[2(1+n)^2]=D/[2(M_{CCM})^2] \quad (32)$$

The curve of τ_{LB} is plotted in Fig. 10. Once the τ_{Lm} is higher than boundary curve τ_{LmB}, the proposed converter operates in CCM.

The voltages across circuit elements are given along with the currents in the Fig. 11 below.

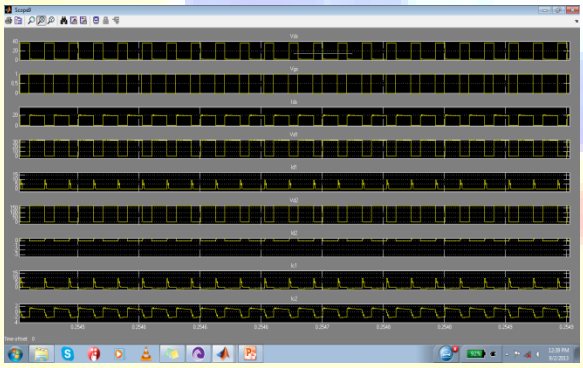

Figure11: Voltages and currents across elements

The output voltage across the proposed converter is given in the Fig. 12 below.

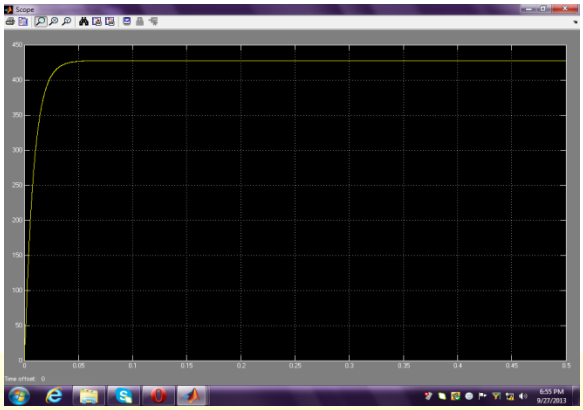

Figure12: Output voltage across proposed converter

VI. CONCLUSION

Since the energy of the coupled inductor's leakage inductor has been recycled, the voltage stress across the active switch *S*1 is constrained, which means low ON-state resistance *R*DS (ON) can be selected. Thus, improvements to the efficiency of the proposed converter have been achieved. The switching signal action is performed well by the floating switch during system operation; on the other hand, the residential energy is effectively eliminated during the non operating condition, which improves safety to system technicians. From the prototype converter, the turns ratio $n = 5$ and the duty ratio D is 55%; thus, without extreme duty ratios and turns ratios, the proposed converter achieves high step-up voltage gain, of up to 13 times the level of input voltage. The experimental results show that the maximum efficiency of 95.3% is measured at half load, and a small efficiency variation will harvest more energy from the PV module during fading sunlight.

REFERENCES

1. T. Shimizu,K.Wada, andN.Nakamura, "Flyback-type single-phase utility interactive inverter with power pulsation decoupling on the DC input for an AC photovoltaic module system," *IEEE Trans. Power Electron.*, vol. 21, no. 5, pp. 1264–1272, Jan. 2006.

2. J. J. Bzura, "The ac module: An overview and update on self-contained modular PV systems," in *Proc. IEEE Power Eng. Soc. Gen. Meeting*, Jul. 2010, pp. 1–3.

3. C. Rodriguez and G. A. J. Amaratunga, "Long-lifetime power inverter for photovoltaic ac modules," *IEEE Trans. Ind. Electron.*, vol. 55, no. 7, pp. 2593–2601, Jul. 2008.

4. S. B. Kjaer, J. K. Pedersen, and F. Blaabjerg, "A review of single-phase grid-connected inverters for photovoltaic modules," *IEEE Trans. Ind. Appl.*, vol. 41, no. 5, pp. 1292–1306, Sep./Oct. 2005.